JOURNAL OF GEOPHYSICAL RESEARCH, VOL. 105, NO. A12, PAGES 27,179–27,193, DECEMBER 1, 2000

Measurements of the solar soft X-ray irradiance by the Student Nitric Oxide Explorer: First analysis and underflight calibrations

S. M. Bailey,[1] T. N. Woods,[2] C. A. Barth,[2] S. C. Solomon,[2]
L. R. Canfield,[3] and R. Korde[4]

Abstract. Beginning on March 11, 1998, the Student Nitric Oxide Explorer (SNOE) satellite has made daily observations of the solar soft X-ray irradiance. These measurements are carried out by a multichannel photometer system. The spectral range between 2 and 20 nm is covered by three channels with bandpasses of 2 – 7 nm, 6 - 19 nm, and 17 – 20 nm respectively. Absolute sensitivities were measured preflight using the Synchrotron Ultraviolet Radiation Facility of the National Institute of Standards and Technology. The results of the first 1.5 years of SNOE solar measurements are presented. During this time period the $F_{10.7}$ solar index varied between 80 and 250 x 10^{-22} W m^{-2} Hz^{-1} and the 81-day average of the $F_{10.7}$ solar index varied between 100 and 175 x 10^{-22} W m^{-2} Hz^{-1}. The solar irradiances in the 2 - 7 nm interval varied between 0.3 and 2.5 mW m^{-2}, while the irradiances in the 6 – 19 and 17 – 20 nm intervals varied between 0.5 and 3.5 and 1.0 and 3.5 mW m^{-2}, respectively. The measured irradiances are correlated with the $F_{10.7}$ solar index with a correlation coefficient of ~0.9 in all three bandpasses. For the levels of activity observed so far the SNOE measurements are typically a factor of 4.0 larger than the irradiances predicted by the *Hinteregger et al.* [1981] empirical model (hereafter the Hinteregger model). This fact and a long-term trend in the ratio of SNOE measurements to Hinteregger model predictions show that the Hinteregger model underpredicts the long-term variability in the solar soft X-ray irradiance. It is shown that other empirical models provide a reasonable representation of the 27-day variability but also underpredict the magnitude and long term variability. A sounding rocket measurement made on November 2, 1998, by the Thermosphere Ionosphere Mesosphere Energetics and Dynamics Solar EUV Experiment prototype instrument using the same technique measured the solar irradiance in similar wavelength bands and produced results that are in good agreement with the SNOE measurements.

1. Introduction

The solar irradiance in the wavelength range below 30 nm (soft X-rays) is deposited mostly into the lower thermosphere at altitudes between 100 and 150 km. This energy photoionizes the neutral constituents of the atmosphere and participates in the formation of the ionosphere. The photoelectrons created in this process interact further with the neutrals, leading to excitation, dissociation, and further ionization. Understanding these processes and their variability is hampered by the lack of solar irradiance measurements below 30 nm. *Lean* [1987] reviewed the history of solar irradiance measurements and the current understanding of the ultraviolet spectrum and its variability. The majority of knowledge on solar soft X-ray irradiance comes from Air Force measurements on the Atmospheric Explorer (AE) satellites and sounding rockets [*Hinteregger et al.*, 1981; *Torr and Torr*, 1985] as well as several other sounding rocket programs [see *Manson*, 1976; *Feng et al.*, 1989 and references therein; and *Bailey et al.*, 1999a], the Explorer series of satellites [*Gibson and Van Allen*, 1970], a Naval Research Laboratory satellite program [*Kreplin*, 1970; *Kreplin and Horan*, 1992], and the CORONAS-I [*Kazachevskaya et al.*, 1998] mission. Many of the measurements other than those of AE and some of the rocket experiments focused on shorter wavelengths than are discussed here. More recent observations in wavelength bandpasses that partially overlap the Student Nitric Oxide Explorer (SNOE) bandpasses are currently being made by the Solar Extreme Ultraviolet Monitor (SEM) on the Solar and Heliospheric Observatory (SOHO) [*Judge et al.*, 1998] and the Yohkoh solar imaging experiment [*Acton et al.*, 1999]. The measurements to date are sparse and do not cover the full range of solar activity.

The limited amount of solar data make proxy models of the solar variability necessary. The first widely used model was the empirical model of *Hinteregger et al.* [1981] (hereafter referred to as the Hinteregger model). The proxies are the chromospheric H I Lyman ß (102.6 nm) and the coronal Fe XVI (33.5 nm) emissions. As measurements of these emissions are not typically available, they are correlated with

[1]Center for Atmospheric Sciences, Hampton University, Hampton, Virginia.
[2]Laboratory for Atmospheric and Space Physics, University of Colorado, Boulder.
[3]Physics Laboratory, National Institute of Standards and Technology, Gaithersburg, Maryland.
[4]International Radiation Detectors, Torrance, California.

Paper number 2000JA000188.
0148-0227/00/2000JA000188$09.00

the Ottawa (or currently Penticon) 10.7 cm radio flux (F10.7) and its 81-day average which have been available on a daily basis since 1947. The Hinteregger model is referred to as SERF 1 by the Solar Electromagnetic Radiation Flux subgroup of the World Ionosphere-Thermosphere Study.

Following the work of Hinteregger *et al.*, Richards et al. [1994] developed a proxy model called EUVAC which increased the solar soft X-ray irradiances by a factor of 2 to 3 as compared to the SERF 1 model. *Tobiska and Barth* [1990] developed a model of the solar irradiance, named SERF 2. *Lean* [1990] compared the results of SERF 1 and SERF 2 over timescales of the 27-day solar rotation and the 11-year solar cycle and concluded that the two models predicted significantly different variability. *Tobiska* [1991] consequently revised the SERF 2 model. The new version was compared to SERF 1 and SERF 2 by *Buonsanto et al.* [1992], who concluded that, at soft X-ray wavelengths the Tobiska [1991] model produced more ionization in the ionosphere and therefore more irradiance than SERF 1. *Tobiska and Eparvier* [1998] updated the earlier Tobiska models with a focus on soft X-ray irradiances. Tobiska and coworkers have continued to update and expand their model as more data sets have become available. The latest version, SOLAR2000 (V1.03), is under development and will cover the spectral range 1 to 1,000,000 nm over the time period from 1947 until the present [*Tobiska et al.*, 2000].

Atmospheric studies have highlighted the need for better knowledge of the magnitude and variability of the solar soft X-ray irradiance. *Richards and Torr* [1984, 1985] studied the consistency of photoelectron measurements and calculations using AE measurements of the solar soft X-ray irradiance. They found agreement in the calculated and observed ionospheric photoelectron fluxes if they scaled the solar irradiance below 25 nm by approximately a factor of 2. *Barth et al.* [1988] and *Siskind et al.* [1990] found that large soft X-ray irradiances (relative to reported measurements referred to above) were required to explain nitric oxide densities observed by sounding rockets and by the Solar Mesosphere Explorer (SME). They also found that an assumed order of magnitude variability of solar soft X-ray irradiances in the wavelength range 2 to 5 nm reproduced the large changes in nitric oxide densities seen by SME. *Siskind et al.* [1995] used a more efficient model for photoelectron production and still concluded that larger soft X-ray irradiances were required to explain the SME measurements. A complete summary of the discrepancies between reported solar soft X-ray irradiances, empirical models, and the irradiances required to explain observations of the Earth's atmosphere is given by *Solomon* [1991].

Previous work has demonstrated that the region of the solar spectrum responsible for most photoelectrons lies at and below 30.4 nm [*Richards and Torr*, 1984, 1985]. The 30.4 nm emission comes from the solar transition region, whereas emissions short of 30.4 nm are from the solar chromosphere, transition region, and corona. Chromospheric emission variability is better understood than coronal variability; chromospheric emissions at longer wavelengths have been observed more often, and these emissions typically vary similarly over the solar cycle. *Timothy and Timothy* [1970] correlated the 30.4 nm irradiance measured by the OSO 4 with both the Zurich sunspot number and the $F_{10.7}$ index. More recently, *Judge et al.* [1998] and *Ogawa et al.* [1998] have published measurements of the 30.4 nm irradiance from the SOHO satellite.

Since the AE-E measurements, there has been little data to add to our understanding of the magnitude and the variability of the solar soft X-ray irradiance. The poor reflectivity of most materials in the soft X-ray region makes it difficult to use conventional grating spectrometers. Thus we have developed photometers as an alternative method. Photometry, however, requires the use of filters for wavelength selection. In the soft X-ray region, thin-film foils are often used as filters. The difficulty with foil filters lies in their tendency to develop pinholes that transmit the much brighter longer-wavelength sunlight. *Ogawa et al.* [1990] measured the solar extreme ultraviolet (EUV) and soft X-ray irradiance from a sounding rocket using a photodiode with a thin aluminum coating as well as an aluminum foil filter. By subtracting a constant background from their data due to pinholes and other light leak problems, they were able to conclude that the measured current from the photodiode, most sensitive in the range 17 to 80 nm, was consistent with their other measurements of the solar irradiance from 5 to 50 nm with a helium ionization chamber. The measurement described here also uses photodiodes to measure solar soft X-ray irradiance. For this work, there are no foils; all filter materials are deposited directly on the photodiode. In this paper we describe the development of these soft X-ray photometers along with their data and results from flight on the Student Nitric Oxide Explorer (SNOE).

SNOE was launched on February 27, 1998, into a 556 km near-circular Sun-synchronous orbit with an average local time of 10:30. It is a spinning satellite rotating at 5 rpm. Details of the mission, the scientific objectives, the spacecraft, its subsystems, and the instrumentation can be found in *Solomon et al.* [1996] and *Bailey et al.* [1996]. One of the three science instruments on SNOE is designed to measure the solar soft X-ray irradiance from 2 to 20 nm. The goal of this paper is to describe the measurement technique, the data analysis procedures, results from the first 1.5 years of measurement, and the results of a sounding rocket underflight calibration. Preliminary results from the first 131 days of SNOE have been presented by *Bailey et al.* [1999b]. The results here incorporate updated calibration data and supersede those results as described below.

2. Instrumentation

The Solar X-ray Photometer (SXP) on the SNOE spacecraft performs photometric measurements of the solar soft X-ray irradiance in select wavelength channels. The channels consist of X-ray sensitive photodiodes with thin films deposited directly onto the active areas. *Ogawa et al.* [1990] and *Bailey et al.* [1999a] describe solar irradiance measurements using this technique from sounding rockets. An earlier description of the SNOE SXP was presented by *Bailey et al.* [1996]. We review the instrument here.

The detectors for the SXP are silicon XUV photodiodes that are available commercially and discussed in detail by *Korde and Geist* [1987], *Korde et al.* [1988], and *Canfield et al.* [1994]. Their response at short wavelengths is near the theoretical response for silicon. The sensitivity of an uncoated diode is ~1 electron per photon at 340 nm and increases proportionally at a rate of 1 electron per 3.63 eV of photon

Table 1. SNOE Solar X-ray Photometer Photodiodes

Bandpass, nm	Coating Material	Coating Thicknesses, nm	Signal From Within Bandpass (low to high solar activity)
2 - 7	Ti/TiO	220/100	85 - 91 %
6 - 19	Zr/Ti/C	120/15/70	89 - 82 %
17 - 20	Al/C	210/80	53 - 43 %

energy [*Korde and Canfield*, 1989]. Thus, at 10 nm, there are ~34 electrons per photon. The sensitivity has been shown to be highly stable for large radiation fluences [*Canfield et al.*, 1989]. The National Institute of Standards and Technology (NIST) uses these photodiodes as secondary standards in the 5 to 254 nm spectral region. These Si photodiodes are similar to those flown previously by *Ogawa et al.* [1990] and *Bailey et al.* [1999a].

The photometer bandpass is determined from thin-film filters deposited directly on the photodiode in the wafer form [*Canfield et al.*, 1994; *Bailey*, 1999a, 1999b]. The particular material and thickness in conjunction with the uncoated photodiode response determine the wavelength region of sensitivity for each photometer. Each coating is designed to provide a narrow band of transmission when folded in with the bare photodiode sensitivity. In particular, the coatings must be thick enough to block any contribution from the much brighter long-wavelength spectrum of the Sun. The use of three photometers with different filters yields the desired wavelength coverage. Note that the SNOE compliment of photodiodes consists of four coated photodiodes, three of which are analyzed in this work, and one uncoated diode, which is used for calibrations described later. The combination of bare photodiode sensitivity, coating materials, and thicknesses of those materials determine the passband for each channel. The SNOE compliment of photodiodes is listed in Table 1 along with the coating materials, their thicknesses, and wavelength range to which they are primarily sensitive. These ranges are determined by convolving the sensitivity of the coated diode with a solar reference spectrum. This topic will be described in further detail later in the paper. The SNOE compliment of diodes covers the full range from 2 to 20 nm.

A fourth coated photodiode flown on the SNOE SXP but not listed in Table 1 is coated with Sn. Results from this diode are not described in this paper. The data from this channel do not show a clear signal due to solar soft X-rays. We hypothesize that the active area of this photodiode is not properly connected to spacecraft ground owing to the presence of SnO_2 on the surface of the coating. These connections are important because they provide a path for any charge collected by the surface of the diode to be removed from the circuit. Signals from the Sn channel are indicative of significant charge buildup on the detector and have prohibited any solar irradiance information from being obtained by that channel.

The electronics for the SXP are simple and are designed for a large dynamic range. The current from the photodiode is converted to a voltage through an operational amplifier. A voltage to frequency converter then translates this voltage into a system of digital pulses such that the frequency is proportional to the original current. The pulses are counted within the instrument over programmable periods. For all data analyzed in this work the integration period is 62.8 ms. The pulse counting method allows for a large dynamic range as well as a much smaller susceptibility to noise in the measurements. The range of measurable currents for this electrometer system are 1×10^{-2} to 2×10^{-8} ampere, producing frequencies of 50 Hz to 1 MHz.

Calibrations of the coated photodiodes were performed prior to launch using the Synchrotron Ultraviolet Radiation Facility (SURF II) at the National Institute for Standards and Technology at wavelengths longer than 5 nm [*Canfield*, 1987]. In order to enhance the accuracy of the calibrations and extend the wavelength coverage below 5 nm, the sensitivity is modeled based on the known sensitivity of a bare photodiode [*Korde and Canfield*, 1989; *Canfield et al.*, 1994] and the calculated transmission of the thin-film filters. The modeled sensitivity is used in the data processing. Figure 1 shows the results of both the measured calibrations and the modeled predictions for each of the SNOE photodiodes. The measurements and the model predictions agree to within 5% at the primary wavelengths where the diodes are most sensitive. The NIST measurements have 1σ uncertainties typically less than 5%. In Figure 1, the 2σ uncertainties are shown for the Ti-coated photodiode. The uncertainties are not shown for the other diodes because the uncertainties are smaller than the symbols used in the plot.

It should be noted that the absolute sensitivities of the coated photodiodes alone do not determine the bandpasses of a given channel. Because the solar spectrum is not a smooth continuum but rather a complicated line spectrum, the structure of the solar spectrum must be convolved with the absolute sensitivity of a given channel in order to determine what region of the solar spectrum the current from the photodiode represents. This point is considered further, and such convolutions are shown in Section 4.

When observing the Sun at soft X-ray wavelengths with photodiodes, long wavelength (i.e., visible light) contributions to the measured signal must be accounted for. These contributions are present because the bare photodiodes are nearly as sensitive to visible light as they are to soft X-rays while the solar spectrum is many orders of magnitude brighter. The photodiode coatings are designed to be thick enough to block visible light; however, microscopic pinholes in the coatings pass enough visible light that they produce a significant signal that must be subtracted from the data. This subtraction is made possible by the use of a fused silica window. A door mechanism on the SXP moves the fused silica window in front of the photometer channels. The fused silica passes UV and visible radiation but not soft X-ray or EUV. Therefore measurements made with the door closed give the magnitude of background signal that is due to long-wavelength radiation and any dark current. A correction must be made as the transmission of fused silica is slightly less than 100%. The transmissions of the filters are measured in the

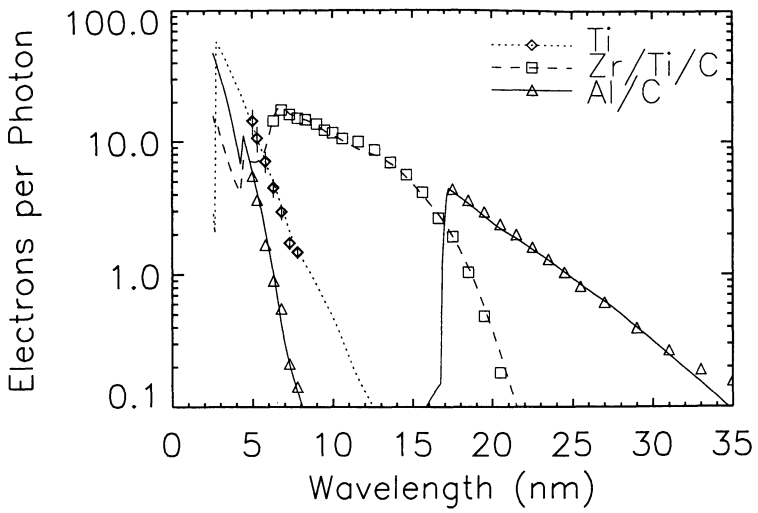

Figure 1. Sensitivity of the coated SNOE photodiodes. Symbols are measurements made at the Synchrotron Ultraviolet Radiation Facility. Vertical lines on the Ti values indicate 2σ uncertainties for those measurements. The uncertainties for the other photodiodes are not shown because they are smaller than the sizes of the plotting symbols. The lines through the symbols are the modeled sensitivities based on the sensitivity of a bare photodiode and the transmissions of the thin film coatings.

laboratory with a tungsten lamp and are typically ~94% at visible wavelengths. Degradation of the fused silica window in space is expected to be minimal; nonetheless, one uncoated SXP photodiode is used to measure the visible transmission of the window.

3. Solar Observations

The SNOE satellite is in a Sun-synchronous orbit with an average local time of 10:30. The satellite spins about an axis perpendicular to the orbit plane. The SXP is mounted within the satellite to view 22.5° away from the orbital plane as the satellite spins. Thus, during the dayside portion of each orbit the SXP scans across the Sun in the axis parallel to the orbit plane. During each scan the Sun appears at a constant angle in the plane perpendicular to the orbital plane. This angle varies as the angle between the Sun and the orbital plane, the β-angle, varies. The deviation of the β-angle from 22.5° can be as large as 10° over the year owing to effects produced by the eccentricity of the Earth's orbit around the Sun and the obliquity of the Earth. Thus a large field of view is required for the Sun to be measured each day of the year. The field of view is defined by two apertures placed in front of each photodiode. The outer aperture is 0.32 cm in diameter and thus defines an active area of 0.08 cm^2. The inner aperture is larger and placed at a distance to allow a field of view of ±35°. This field of view is more than adequate to allow solar irradiance measurements to be made daily on the spinning satellite.

A quadrant diode Sun sensor is co-aligned with the instrument channels. This sensor has an accuracy of 0.25° over a range of ±35° in each of two axis. The Sun sensor is used to determine the location of the Sun in the field of view of the SXP. Knowledge of the Sun position is important in subtracting the visible light background as will be shown later.

Because SNOE is a spinning satellite, the SXP scans the Sun in one axis during each spin on the daytime portion of the orbit. Data are recorded during only a portion of each orbit. For design efficiency, data storage on all SNOE instruments is triggered to Earth Horizon Crossing Indicators (HCIs) so that storage is initiated after a programmable delay period following the HCI trigger pulse. In this implementation the data recording does not capture the Sun during all of the daytime portion of the orbit. The delay is programmed so that the Sun is at the center of the stored scan during that part of the orbit when the Sun is closest to the zenith of the spacecraft. For all of the data shown in this work, 12 samples of 62.8 ms duration are recorded per satellite spin. For each orbit, ~480 samples are recorded with the Sun within ±15° of the instrument line of sight.

Routine measurements with the SXP began on March 11, 1998. The nominal operating mode for the SXP is to open the door and expose the photodiodes to X-ray irradiation during the dayside portions of four orbits each day. The rest of the time, the door is closed in order to ensure that any degradation occurs with the window, where degradation is monitored, and not within the photodiodes themselves.

4. Data Reduction to Irradiance Units

The measurement samples are sorted according to the position of the Sun in the field of view. The visible light contributions to the measurements are subtracted, and the resulting current is then converted into solar irradiance units. Each of these steps is now described.

An individual observing period is considered to be a continuous period during which the door is open. As mentioned above, ~480 individual samples for each channel are taken during such a period. The spacecraft spin dictates that the SXP scans along the Sun in an axis parallel to the orbital plane. For a nominal β-angle of 22.5° the Sun will be

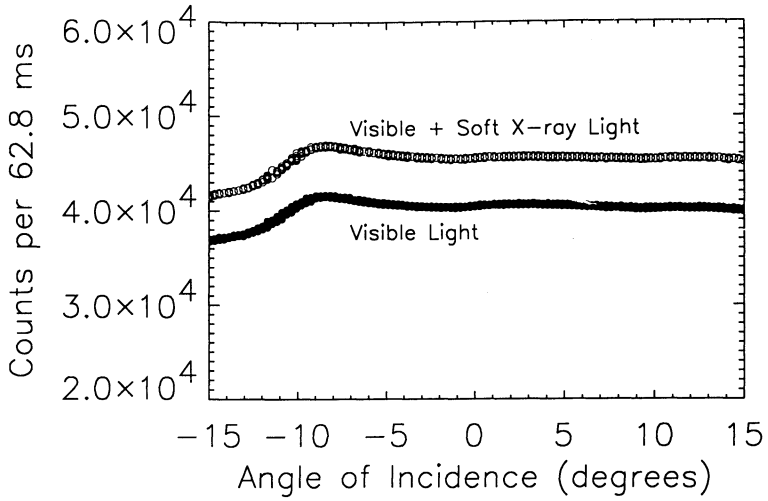

Figure 2. Each measurement made while the Sun was within ±15° of the Solar X-ray Photometer line of sight is shown for March 21, 1999 for the Zr/Ti/C photodiode. These values are shown as a function of incidence angle (parallel to orbit plane) relative to the instrument line-of-sight. The filled circles are measurements made while the fused silica window was in front of the photodiodes. The open circles are measurements made while the fused silica window is removed. The difference between the two is indicative of the solar soft X-ray signal. The visible light response of the instrument as a function of angle is affected by a microscopic pin hole in the coating on one side of the photodiode. The signal due to visible light is enhanced when light is shined directly upon the defect.

centered in the axis perpendicular to the orbital plane. However, the β-angle varies by as much as ±10° over a year. Thus, from orbit to orbit the Sun moves slightly in the perpendicular axis. Knowledge of the position of the Sun within the field of view is important for two reasons. First, the thickness of the coatings as seen by the incident radiation varies according to the secant of the incidence angle. For all incidence angles under consideration in this paper (≤15°) this effect is small; however, if the full field of view of the instrument is used, this effect would be important. The second reason for requiring the incidence angle is that the magnitude of the visible light signal is strongly dependent on incidence angle. This dependence is because the visible light signal is due to pin holes in the coatings that are not spread uniformly across the active area. In fact, they tend to appear in the outer edges of the photodiode and can cause large increases in the visible light signal for angles of incidence near the edges of the field of view. In addition, the visible signal when the fused silica window is present in front of the photodiodes is due to reflections from the window itself. The fraction of visible light due to reflections is measured prior to flight as a function of angle and is incorporated in the data reduction.

Figure 2 shows all of the measurements made on March 21, 1999. The measurements are plotted as a function of position of the Sun in the field of view along the orbital plane. The lower measurements are those made with the SXP door closed and thus are all visible light measurements. The upper measurements are made with the door open and thus are visible plus soft X-ray measurements. The structure in the visible light signals at –9° is due to a microscopic pin hole on one side of the active area. The difference between measurements made with the door open and the door closed is discernable even at this angle and all measurements shown in Figure 2 (i.e., all measurements within ±15° of the instrument line of sight) are used in the analysis.

Removal of the visible light contribution to the measured current is accomplished by subtracting a door-closed (i.e., window in front of the photodiode) measurement from a door-open measurement in the following way:

$$C\mathrm{SXR}_i = C_{\mathrm{open}_i} - \frac{C_{\mathrm{closed}_i}}{T_i}. \quad (1)$$

The subscript i denotes channel, C_{SXR} denotes counts per integration period, which are due to solar soft X-rays, C_{open} denotes measured counts per integration period when the door was open, and C_{closed} denotes measured counts per integration period when the door was closed. The transmission T_i of the window is determined for each observation from the ratio of door-closed and door-open measurements from the uncoated photodiode denoted with a subscript u,

$$T_i = \frac{C_{\mathrm{closed}_u}}{C_{\mathrm{open}_u}} f_i. \quad (2)$$

The factor f_i is the preflight-measured factor that accounts for reflections from the window back onto the diode surface. As described above, the visible light component of any measurement is dependent on the location of the Sun in the field of view; therefore, there is an angular dependence in each of the variables that is not explicitly written into the above equations. Prior to performing the subtraction, all door-open and door-closed measurements are placed in a two-dimensional array (parallel and perpendicular to the spacecraft orbit plane) with 1° bins. The above algorithm is

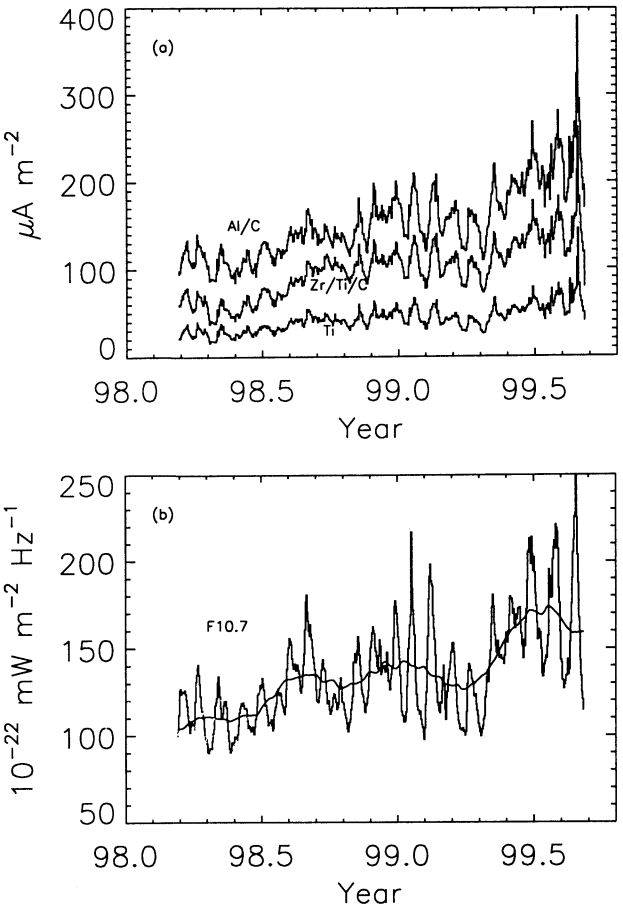

Figure 3. (a) Daily soft X-ray current measurements for the first 1.5 years of the SNOE mission. Currents are shown in units of microamperes per m^2 for each of the three SNOE SXP channels. (b) Values of the solar 10.7 cm irradiance ($F_{10.7}$) for the time period of the measurements shown in Figure 3a. The solid line is the 81-day average of the $F_{10.7}$.

applied on each bin, and the results are then averaged. The door-closed measurements are the average of the visible light measurements made in adjacent orbits.

The remaining signal after subtracting the visible light signal is then converted to current units, microamperes per m^2, using the conversion factor measured prior to launch and the known active area of the photodiode. The resulting currents, due only to solar soft X-ray irradiance, are shown for each of the SNOE photodiodes in Figure 3a. The currents vary from about 20 to nearly 400 μA m^{-2}. The 27-day periodicity due to the Sun's rotation is obvious as is a general increase in signal with time. These current measurements are now ready to be interpreted for determining the solar soft X-ray irradiance. The $F_{10.7}$ index provides a reference for the level of solar activity and is shown in Figure 3b for the time period of the measurements shown in Figure 3a.

The data are now converted into irradiance units. In order to perform this conversion a solar reference spectrum and the sensitivity of the photodiode are convolved and integrated to produce a reference current. The ratio of the measured current to the reference current is defined as the scaling factor for the reference spectrum over the bandpass of the photodiode. The scaling factor is calculated according to:

$$\mathrm{SF}_i = \frac{I_{\mathrm{SXR}_i}}{I_{\mathrm{ref}\,i}} = \frac{I_{\mathrm{SXR}\,i}}{\sum_j S_i(\lambda_j) F(\lambda_j)}, \tag{3}$$

where SF_i is the scale factor for channel i, $I_{\mathrm{SXR}i}$ is the soft X-ray current measured by channel i, $I_{\mathrm{ref}i}$ is the soft X-ray current predicted by the reference spectrum, $S_i(\lambda_j)$ is the sensitivity of channel i at wavelength j, and $F_i(\lambda_j)$ is the model irradiance at wavelength j. Note that the full reference spectrum is used in calculating the reference current. In order to calculate irradiance, the scaling factor is applied to the reference spectrum and the scaled spectrum is integrated over the photodiode's bandpass. The photodiode bandpasses are described below. This process is done for each photodiode individually. The results are reported in energy units (W m^{-2}). Energy units are optimal for the SXP results because a silicon photodiode current is proportional to the impinging energy flux (1 electron hole pair per 3.63 eV photon energy). Thus the effect of uncertainties in shape of the reference spectrum is greatly reduced when values of bandpass integrated energy flux are reported.

Figure 4 shows the convolution of the SNOE photodiode sensitivities with the SC#21REFW solar minimum reference spectrum of *Hinteregger et al.* [1981]. This reference spectrum is at a resolution of ~0.1 nm; however, it is shown in Figure 4 in 1 nm bins. In practice, the full model resolution is used. Figure 4 also shows the results of the convolution of sensitivity and solar spectrum for a high solar activity reference spectrum. This spectrum is obtained from the Hinteregger model assuming a value of 250 x10^{-22} W m^{-2} Hz^{-1} for both the daily and the 81-day average of the F10.7. The photodiode sensitivities, convolved with the reference spectrum as shown in Figure 4, show which wavelengths generate the bulk of the soft X-ray current generated by each photodiode when viewing the Sun. It is these convolutions that are used to determine the bandpass of each photometer channel. The convolutions are shown in units of percent of total current in 1-nm intervals. Thus, for the Ti-coated photodiode, 32% of the total signal comes from solar irradiance in the 5 - 6 nm interval and 85% in the 2 - 7 nm interval. Note that while some of the current is produced at wavelengths longer than 7 nm, we declare the photodiode bandpass as 2 - 7 nm. This is because for longer wavelengths, significant changes in the solar spectrum produce negligible changes in the total measured current, and therefore the measured current may not be indicative of the brightness of the Sun at those wavelengths. In the analysis described above and detailed below, contributions outside the declared bandpass are still considered. The stated bandpass is used as a reference and for reporting of irradiances. For the Zr/Ti/C photodiode, 88% of the current is produced by solar photons in the 6 - 19 nm bandpass. The Al/C receives ~15% of its signal from the bright solar 30.4 nm feature and ~10% from wavelengths less than 10 nm; however, 54% of the Al/C signal comes from the spectral region between 17 and 20 nm. Less than 5% per nm of the signal comes from wavelengths between 20 and 30 nm. Therefore the Al/C photodiode bandpass is declared to be 17 - 20 nm. The contribution to the total signal from the declared bandpass is stated for each

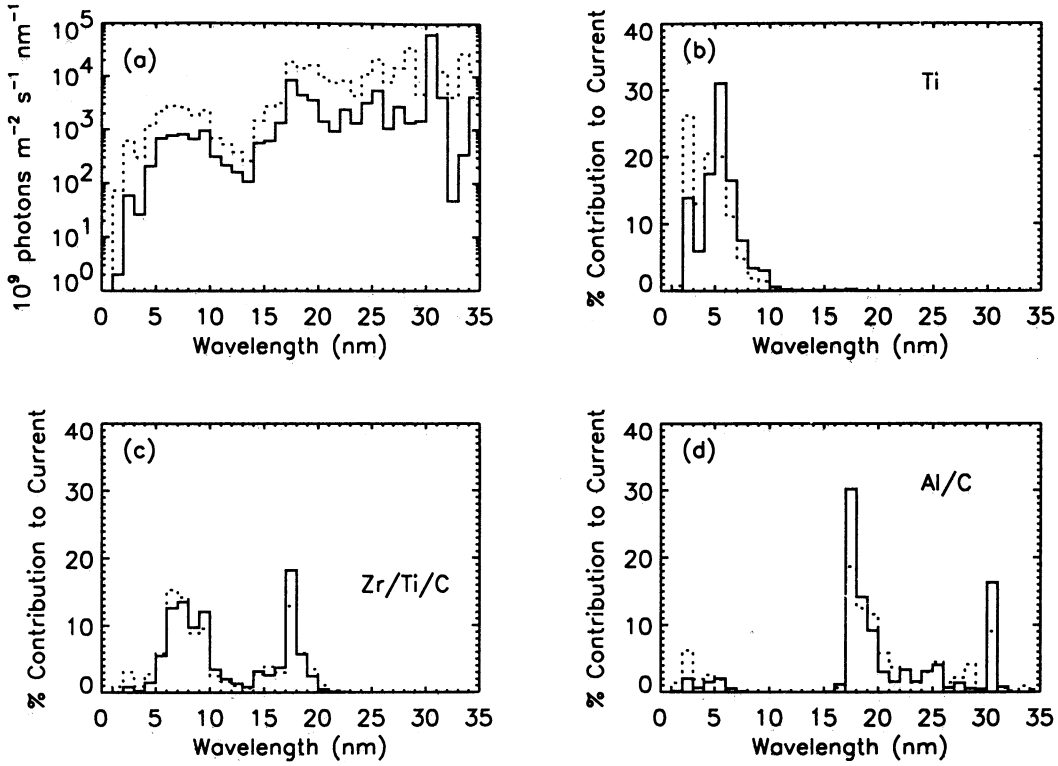

Figure 4. Convolutions of the photodiode sensitivities with a reference solar spectrum. The convolutions are shown in 1-nm bins. (a) The reference spectra used for these examples are shown. The solid line is the SC#21REFW solar minimum reference spectrum; the dotted line is a solar maximum ($F_{10.7}$=250) reference spectrum. See text for details. (b) The Ti photodiode current is produced primarily by 2 – 7 nm solar photons, (c) the Zr/Ti/C current is produced primarily by 6 – 19 nm solar photons, and (d) the Al/C current is produced primarily by 17 – 20 nm solar photons.

photodiode and are shown for high as well as low solar activity in Table 1.

The first analysis of the SNOE data by *Bailey et al.* [1999a] used a single model solar spectrum for each day. This can introduce errors as solar activity rises, and the concentration of solar flux tends to move toward shorter wavelengths (within the bandpasses of the SNOE channels). Our tests have shown that this effect is small (~5%) for the Al/C and Zr/Ti/C channels but can cause an error of up to 25% for the Ti channel. Thus, for the present work a different solar spectrum for each day is used. This solar spectrum is obtained from the model of *Hinteregger et al.* [1981] and is based on the SC#21REFW solar minimum reference spectrum. The Hinteregger model takes the daily $F_{10.7}$ and the value of the 81-day average of the daily $F_{10.7}$ values as input parameters.

Uncertainties in the derived irradiances from the above procedures are due to uncertainties in the calibrations, errors of line ratios in the assumed solar spectrum, and random errors in the measurements. The random errors play a role four times as the soft X-ray current is the result of a difference measurement (equation (1)) and a ratio (equation (2)). The uncertainties in the calibrations including measurements and the application of the modeled sensitivity are ~10%. Errors in the line ratios of the assumed solar spectrum are estimated to affect the irradiance of the order of 5%. This value is obtained by comparing results using different model solar spectra representative of different levels of solar activity. The largest source of error is the component introduced in subtracting the visible light background. The resulting uncertainty from this source is quantified by examining the standard deviation about the mean current measurement from each observing period. The standard deviation in the Ti-coated photodiode data (2 – 7 nm) is typically ~20% and for the Zr/Ti/C and Al/C photodiode data (6 – 19 nm and 17 – 20 nm) ~10%. All of the above uncertainties are 1σ values. The total root-mean-square uncertainty is on average 23% for the Ti measurements and 15% for the Zr/Ti/C and Al/C photodiodes.

5. Results

The daily average scale factors derived from the irradiance conversion above are shown in Figure 5. It is worth noting again that the scale factors are the ratio of the SNOE measured solar soft X-ray current to the current predicted using the Hinteregger model, which takes into account solar activity. The magnitudes of the scale factors suggest that the measurements are, on average, approximately a factor of 4.0 greater than the Hinteregger model would predict for the Ti and Al/C photodiodes and a factor of 2.5 higher than the Hinteregger model would predict for the Zr/Ti/C photodiode. Note that these results are larger than the preliminary results

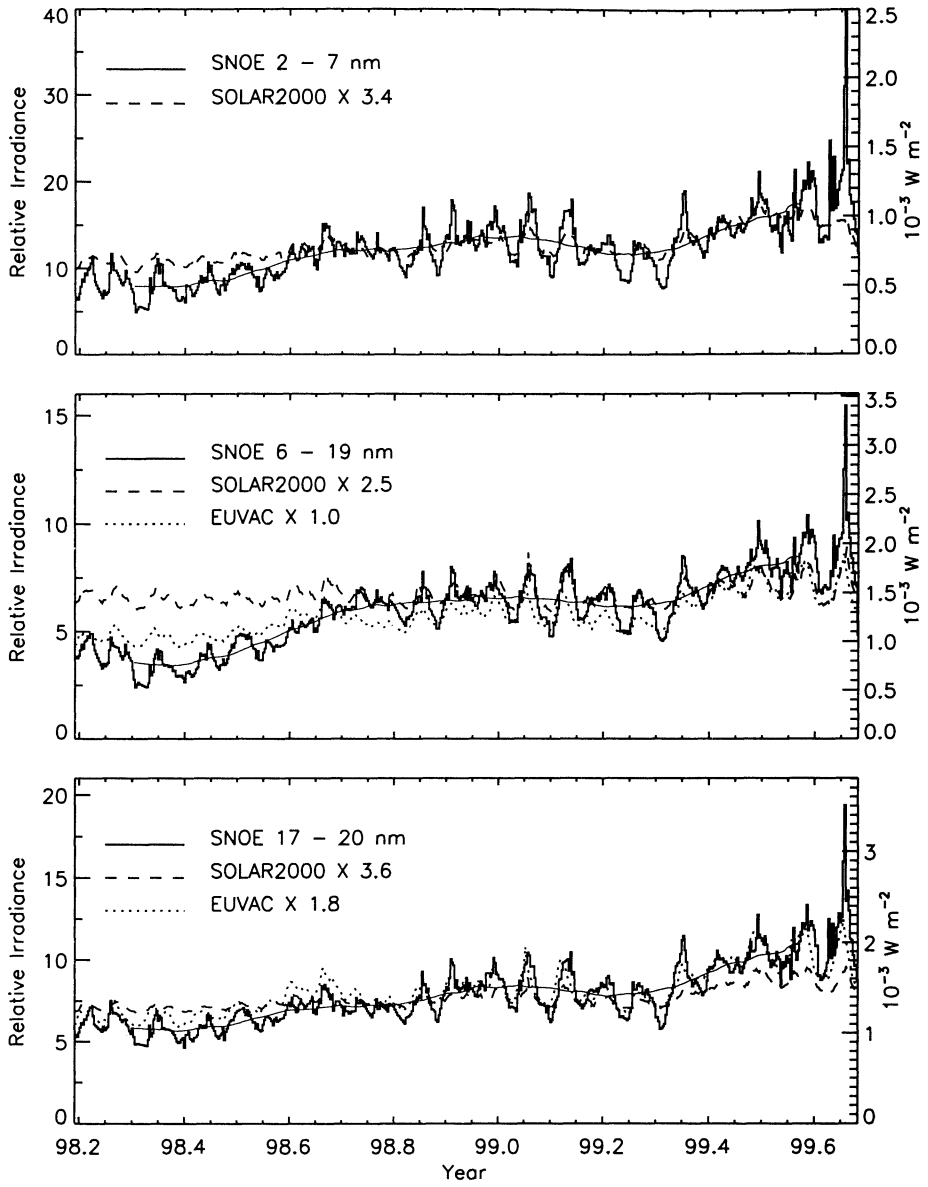

Figure 5. Ratios of measured current to that current predicted by the model solar spectrum appropriate to each measurement. These ratios are indicative of the relative difference between the measured solar irradiance and the Hinteregger model solar irradiance. The solid line is a linear fit to the ratios and shows that the Hinteregger model does not fully capture the long-term variability in the solar irradiance. The dotted line is the average ratio for the SNOE observations.

described by *Bailey et al.* [1999b] owing to updates in the calibration that have been incorporated since that early work. These scale factors show a small long-term trend with smaller scaling factors earlier in the mission during the lowest solar activity. This small trend may be due to the use of $F_{10.7}$ as a proxy in the Hinteregger model, which produces the reference spectrum. The scale factors also show a small 27-day periodicity that tracks the $F_{10.7}$ suggesting that the Hinteregger model slightly underestimates the 27-day variability in the solar irradiance. Figure 5 also includes a linear fit to the scale factors. The slopes in the linear fits indicate that the Hinteregger model underestimates the long-term variability in the solar irradiance by 20% over the time period of the SNOE observations in the 2 – 7 nm and 17 – 20 nm ranges and 60% in the 6 - 10 nm range. It is also seen in Figure 5 that the scatter in the scale factors around the linear fits is greater at the shorter wavelengths. This is mostly because the shorter wavelengths have smaller soft X-ray signals, and thus the noise in the data is greater. Some of this scatter, especially near the beginning and the end of the 2 - 7 nm time series, is also due to the use of $F_{10.7}$ as a proxy in the Hinteregger model.

There are typically four individual solar X-ray measurements per day, and these are averaged to produce a

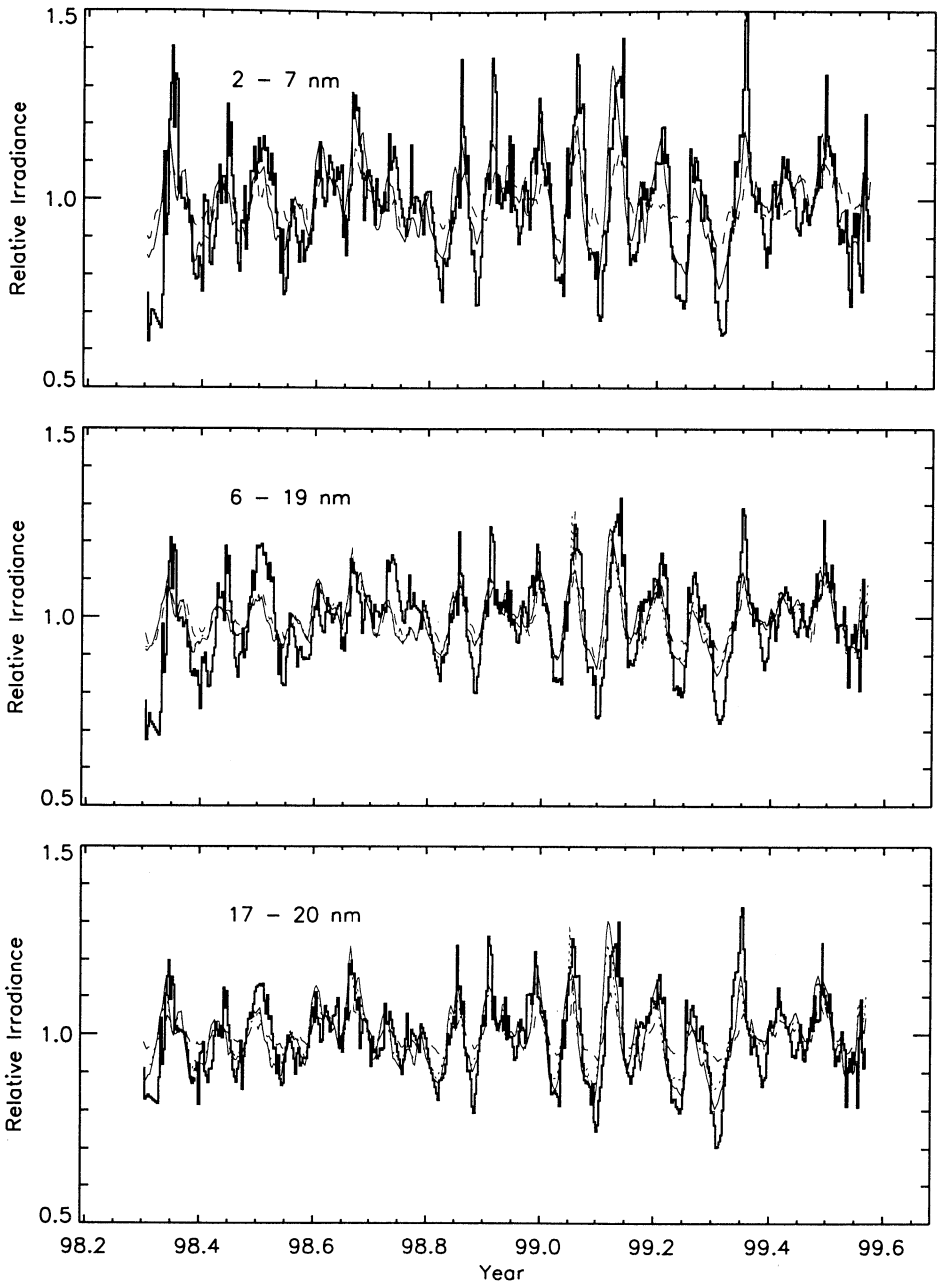

Figure 6. Irradiances derived from the ratios in Figure 5. The irradiances are shown in units of energy flux normalized to the *Hinteregger et al.* [1981] solar minimum values as well as in 10^{-3} W m^{-2}. Also shown are scaled predictions by the SOLAR2000 and EUVAC empirical models. The thin solid line is the 81-day average of the SNOE measurements.

daily result. The daily averaged irradiances for the first 1.5 years of the SNOE mission are shown in Figure 6. Solar flares are identified from the measurements by looking at days when the four individual measurements are very different from one another and the daily average is more than a factor of 3 times larger than the surrounding days. These time periods are examined in the GOES-8 satellite measurements of the solar 0.1 to 0.8 nm flux to verify they are times of flare activity. There are 3 days during the time period covered in Figure 6 that are affected by flares. In Figure 5 and those following, for the 3 days where flares are identified, the SNOE measurements are not shown and in their place is the average of the surrounding days. The flare-affected values are factors of 5 to 10 times the values of the surrounding days. It is not yet known by what factor solar flares increase the solar soft X-ray irradiance. Solar flare data should be analyzed with a different solar spectrum and should be examined by individual observations rather than in daily averages. This analysis will be forthcoming in a later paper.

The results in Figure 6 are presented both in units of

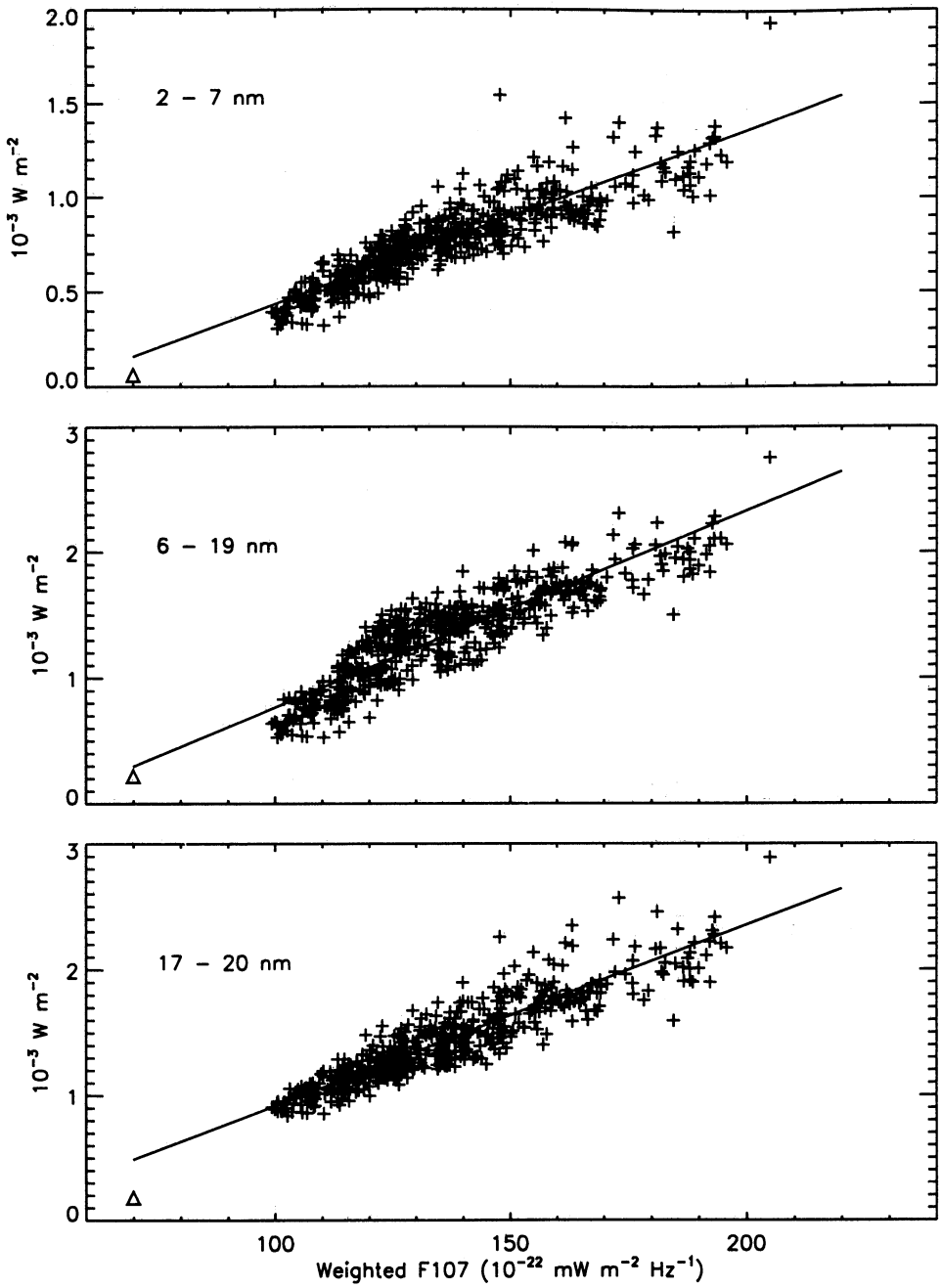

Figure 7. Correlations between the measured solar irradiances and the $F_{10.7}$ solar index. For all three channels the correlation coefficients are near 0.9.

absolute energy flux, mW m^{-2}, and normalized energy flux where the results are normalized to the SC#21REFW [*Hinteregger et al.*, 1981] solar minimum irradiances for the SNOE bandpasses. The smooth curves show the 81-day averages of these values. For the 2 – 7 nm channel the irradiances for the levels of activity during the observation period (81-day average of $F_{10.7}$ between 100 and 175 x10^{-22} W m^{-2} Hz^{-1}) vary between 4.8 and 40 times the Hinteregger solar minimum value, demonstrating variability of a factor of 8.3. The variability decreases with longer wavelength with a maximum to minimum ratio of 6.4 for the 6 - 19 nm daily irradiances and a ratio of 4.2 for the 17 – 20 nm daily irradiances. The 81-day averages show smaller variability with closer agreement among the channels. The 81-day average of the 2 – 7 nm irradiances varies by a factor 2.2, the 6 – 19 nm irradiances by 2.5, and the 17 – 20 nm irradiances by 1.9.

Also shown in Figure 6 are predicted solar irradiances from the EUVAC and SOLAR2000 (V1.03) empirical models. The EUVAC model considers wavelengths greater than 5 nm and so is not compared to the 2 – 7 nm channel. This model produces photon irradiances in wavelength bins as large as 5

Table 2. Linear Fit Results

Wavelength Interval, nm	Correlation Coefficient	Slope, mW m^{-2} per $F_{10.7}$	Intercept, mW m^{-2}
2 - 7	0.87	0.0093	-0.49
6 - 19	0.89	0.016	-0.80
17 - 20	0.91	0.014	-0.52

nm. The photon irradiances were converted into energy units and binned in the SNOE bins assuming the spectral distribution of the SC#21REFW reference spectrum. In the 6 – 19 nm bin the EUVAC model agrees very well with the SNOE measurements in magnitude. It predicts a slightly higher irradiance early in the mission during lower solar activity, but is in excellent agreement during later time periods. In the 17 – 20 nm range the EUVAC model very consistently predicts irradiance a factor of 1.8 lower than the SNOE measurements. The SOLAR2000 model predictions are from version 1.03 and are produced in units of energy irradiance at the wavelength resolution of SC21REFW. The model bins are then summed into the SNOE wavelength bins. The SOLAR2000 model underpredicts the measured irradiance in all three wavelength regions. It predicts irradiances lower than the SNOE measurements by factors of 3.4, 2.5, and 3.6 in the 2 – 7 nm, 6 – 19 nm, and 17 – 20 nm ranges, respectively. These factors are averaged over the time period of the SNOE measurements. Figure 6 shows that the disagreement varies slightly with time, showing the SOLAR2000 model also underpredicts the long-term variability.

The 27-day periodicity due to solar rotation is obvious in Figure 6. The SOLAR2000 and EUVAC models appear to do a reasonable job of reproducing the 27-day variability, particularly during the later times periods (i.e., higher levels of solar activity). The 27-day variability is clearly larger at the shorter wavelengths. The average maximum to minimum ratio for 27-day variability in the 2 –7 nm irradiance is 1.8. For the 6 – 19 nm and 17 – 20 nm irradiances the average maximum to minimum ratios for 27-day variability are 1.5 and 1.4, respectively.

The relationship between the SNOE solar soft X-ray irradiances and $F_{10.7}$ values is examined in Figure 7. Here the daily soft X-ray irradiances are plotted versus a weighted $F_{10.7}$ value. The weighted $F_{10.7}$ value is merely the average of the daily and the 81-day average of $F_{10.7}$ for a given day. We have found that the soft X-ray irradiances correlate better with the weighted $F_{10.7}$ and in addition, it is an equal weighting of $F_{10.7}$ and 81-day average of the $F_{10.7}$ that is used as the independent variable in the Hinteregger model. Included in each panel of Figure 7 is a linear fit to the SNOE data. For each of the three SNOE SXP channels the correlation between the weighted $F_{10.7}$ and the soft X-ray measurements is near 0.9. The exact values as well as the fit coefficients are shown in Table 2.

While SNOE began making observations after solar minimum, an approximation of the solar minimum irradiances can be made. Assuming that the linear correlations of Figure 7 extend to solar minimum, then the linear fits can be used to predict solar minimum solar soft X-ray irradiances. It is known that while $F_{10.7}$ tends to reach a threshold near 68 x10^{-22} W m^{-2} Hz^{-1}, the EUV irradiances tend to show continued variability; thus, this method is only accurate to first order. We represent solar minimum conditions by $F_{10.7}$ and the 81-day average of the $F_{10.7}$ equaling 70 x10^{-22} W m^{-2} Hz^{-1}. The predicted solar minimum irradiances for each of the SNOE bandpasses are shown in Table 3, which also shows the solar minimum irradiances for the same bandpasses taken from the SC#21REFW solar spectrum. The SNOE results are ~2.5 times the SC#21REFW values in the 2 – 7 nm and 17 – 20 nm bandpasses and ~1.5 times the SC#21REFW values in the 6 – 19 nm bandpass. The consistent result is then that the SNOE measured irradiances are larger than the Hinteregger et al. values as well as other models and that the difference is larger at higher solar activity.

6. Discussion

During the time period of the SNOE observations in Figure 6 the solar $F_{10.7}$ radio flux varied from ~80 to 250 x10^{-22} W m^{-2} Hz^{-1} as shown in Figure 3b. The 81-day average of the $F_{10.7}$ varied from ~100 to 175 x10^{-22} W m^{-2} Hz^{-1}. Thus the SNOE measurements range from low to moderate solar activity. They do not cover solar minimum or solar maximum conditions. The above work shows that the SNOE solar soft X-ray irradiances are consistently larger than those of the Hinteregger model as well as the EUVAC and SOLAR2000 models. At solar minimum the measurements suggest a solar irradiance 2.5 times the Hinteregger model and at the levels of solar activity during which SNOE has observed, the measurements are approximately a factor of 4.0 larger than the Hinteregger model. These two facts suggest that the Hinteregger model significantly underpredicts the long-term variability of the solar soft X-ray irradiance. The discrepancy is 20% for the 2 – 7 nm and 17 – 20 nm ranges and 60% for the 6 - 19 nm range over the time period of the SNOE measurements. These values would certainly be larger if the full range of solar activity were considered. The models do, however, provide a reasonable representation of the 27-day periodicity. These results are not surprising given that several works [e.g., *Barth et al.*, 1988; *Siskind et al.*, 1990; *Richards et al.*, 1994; and *Bailey et al.*, 1999a] have suggested that a factor of 2 or more discrepancy exists between the true irradiances and those of Hinteregger. As mentioned above, the

Table 3. Solar Minimum Irradiances

Wavelength Interval, nm	SC#21REFW, mW m^{-2}	SNOE SXP, mW m^{-2}
2 - 7	0.063	0.16
6 - 19	0.22	0.30
17 - 20	0.18	0.49

Table 4. Configuration and Results of Rocket Photometers Flown on November 2, 1998

XP No.	Coating (Bandpass)	soft X-ray Current, nA/cm^2	Rocket Irradiance, mW/m^2	Irradiance Ratio of Rocket to Model	Irradiance Ratio of SNOE to Model	Ratio of SNOE to Rocket
1	Ti/C (2-7 nm)	1.1 (2%)	0.52 (15%)	3.4	4.6 (22%) (2-7 nm)	1.4 ± 0.7
2	Ti/Pd (2-10 nm)	1.7 (14%)	0.80 (15%)	3.2	4.6 (22%) (2-7 nm)	1.4 ± 0.7
3	Lyman-α (121.6 nm)	0.18 (3%)	6.7 (12%)	0.8	-	-
5	Ti/Zr/Au (6-12 nm)	0.47 (15%)	0.59 (16%)	3.5	3.6 (16%) (6-19 nm)	1.0 ± 0.2
6	Al/Mn (2-6 nm)	2.8 (4%)	0.46 (25%)	4.4	4.6 (22%) (2-7 nm)	1.0 ± 0.6
7	Cr/Al (28-34 nm)	6.7 (7%)	2.6 (24%)	3.1	-	-
10	Al/Nb/C (17-21 nm)	2.9 (2%)	1.5 (9%)	4.2	4.0 (15%) (17-20 nm)	1.0 ± 0.2
11	Al/Sc/C (17-26 nm)	8.2 (24%)	1.4 (25%)	2.2	4.0 (15%) (17-20 nm)	1.9 ± 0.6

analysis reported here incorporates updated calibration values compared to the preliminary analysis of SNOE Ti photodiode data by *Bailey et al.* [1999b]. The values reported here are approximately a factor of 4 larger than those of *Bailey et al.* [1996b]. In an upcoming paper, the SNOE measurements will be compared to previous sounding rocket measurements such as those compiled by *Feng et al.* [1989] as well as other satellite data.

7. Sounding Rocket Underflight Calibrations

Rocket measurements of the solar soft X-ray irradiance on November 2, 1998, provide a validation of the SNOE solar soft X-ray irradiances. These underflight measurements were made by soft X-ray photometers during the development of the Solar EUV Experiment (SEE) instrument for the NASA Thermosphere-Ionosphere-Mesosphere Energetics-Dynamics (TIMED) mission [*Woods et al.*, 1998, 1999]. The prototype SEE soft X-ray photometers were flown as part of NASA Rocket 36.171 (PI: Don Hassler) to study the solar corona. In addition to the validation of the SNOE solar soft X-ray irradiances, this comparison of the rocket and SNOE solar soft X-ray irradiances provides an indirect validation of the radiometric standards at the German Physikalisch Technische Bundesanstalt BESSY (PTB BESSY) and NIST SURF-II facilities because the rocket photodiodes were calibrated at PTB BESSY (while SURF-II was being refurbished into SURF-III) and the SNOE photodiodes were calibrated at NIST SURF-II.

The SEE's soft X-ray Photometer System (XPS) consists of 12 photodiodes mounted with an 8-position filter wheel. The soft X-ray filters are, like SNOE's, thin metal film coatings deposited directly on the Si photodiodes. The filter wheel contains open apertures, fused silica windows, and blank apertures in order for the XPS to measure the solar soft X-ray signal, solar visible signal, and the photodiode dark current, respectively. The transmissions of the fused silica windows are measured during solar observations by using bare Si photodiodes in the XPS. The configuration of SEE's XPS is described in more detail by *Woods et al.* [1998] and the XPS calibrations are discussed by *Woods et al.* [1999].

The configuration and irradiance results of the soft X-ray photometers for the November 2, 1999, rocket flight are obtained following procedures similar to those described for SNOE and are listed in Table 4. The ratios of the measured irradiances to the Hinteregger model predictions are given in Table 4 and are also plotted in Figure 8. The photodiodes that have a minor visible light correction have the lower measurement uncertainties, which are listed with the soft X-ray current values in Table 4.

The primary contributions to the irradiance uncertainties are the absolute accuracy of transferring the radiometric standard, the uncertainty of the solar spectral distribution used in modeling the irradiance, and the uncertainty of the solar soft X-ray signal after removing the solar visible signal from the photodiode's total signal. The uncertainties for these rocket solar soft X-ray irradiances range from 9% to 25%. The reported accuracy for the PTB BESSY calibrations of the SEE photodiodes is typically 3%. The reported accuracy for the NIST SURF-II calibrations of the SNOE photodiodes is typically 5-10% with the larger uncertainties at the shorter wavelengths. The irradiance uncertainties for the SNOE measurements are mostly due to the errors induced by subtracting the visible light component to produce the soft X-ray signal. The need to improve upon the ratio of the soft X-ray signal to the visible signal was recognized after the SNOE soft X-ray photometers were built, so the next generation of soft X-ray photometers, such as for SEE, have thicker soft X-ray filter coatings. Therefore the irradiance uncertainties for many of the rocket photodiodes are dominated more by the uncertainties of the PTB BESSY calibrations and the uncertainty of the solar spectral distribution used in modeling the irradiance.

Intercomparison of the rocket results and comparison of those results with the SNOE results is done in terms of scaling factors relative to the Hinteregger model. This simplifies the discussion since each photodiode has a different bandpass. The short-wavelength rocket measurements below 12 nm

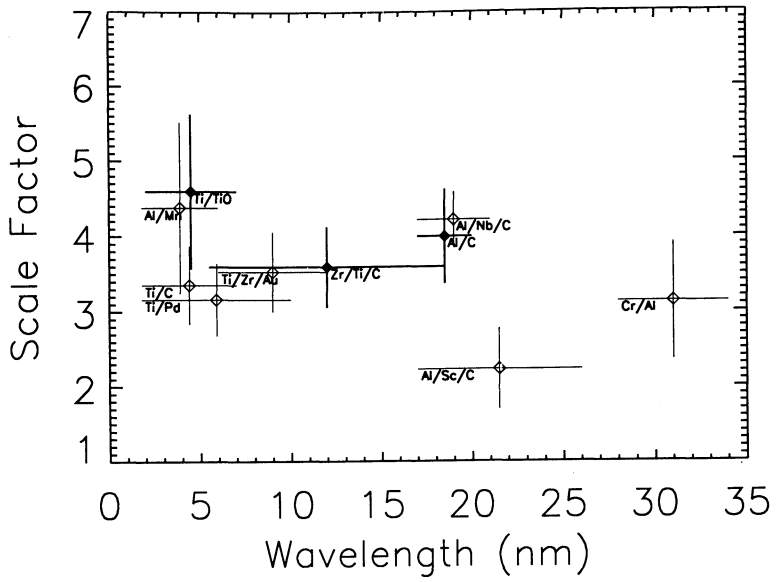

Figure 8. Scale factors for solar irradiance model (see Figure 5) for November 2, 1998. The rocket results are shown as the open symbols with the bandpasses (horizontal bars) and uncertainties (vertical bars) indicated. The SNOE results are shown as closed symbols with thicker lines depicting the bandpasses and the uncertainties.

agree with each other to within their uncertainties. The Al/Mn photodiode result is higher than the other results, but this result agrees within its uncertainty. The longer-wavelength measurements by the Al/Nb/C and Al/Sc/C photodiodes, which have overlapping bandpasses, disagree by a factor of 1.9. The Al/Sc/C photodiode measurement has the larger uncertainty because its visible light correction is large. Any additional analysis of the visible light correction is not likely to change the Al/Sc/C result by more than 25%. In favor of this Al/Sc/C result, past measurements of the 17 - 21 nm region using Al/Sc/C and Al/C photodiodes [*Bailey et al.*, 1999a] have very similar ratios for the measured irradiance to the model predictions. Another source of possible error is the contamination of either photodiode measurement by the bright He II 30.4 nm emission. In particular, if the Al/Nb/C photodiode had more sensitivity at 30.4 nm than expected, then its irradiance reported for 17 - 21 nm would be too large. The calibration for the Al/Nb/C photodiode was only out to 25 nm at PTB BESSY, and the sensitivity for the longer wavelengths was determined using a model of the Al/Nb/C transmission. There is a possibility that the Al/Nb/C photodiode measurement could be contaminated by longer-wavelength emissions; however, this effect is not likely to change the 17 - 21 nm irradiance by more than 20%. There is no clear solution for this discrepancy, so we conclude for now that additional studies and measurements are needed to resolve this discrepancy.

For the SNOE validation, the scale factors of measured current to that predicted from the Hinteregger model are compared for the SNOE and rocket soft X-ray photometers. This comparison is given in Table 4 and Figure 8. In all three SNOE bandpasses the SNOE measurements agree well with at least one of the rocket measurements. At the shorter wavelengths the SNOE measurement is within 5% of the Al/Mn rocket measurement but is ~40% higher than the Ti/C and the Ti/Pd rocket measurements. As shown in Figure 8, however, these discrepancies are within the measurement uncertainties. The SNOE Zr/Ti/C (6 – 19 nm) measurement is in excellent agreement (to within 2%) with the rocket Ti/Zr/Au (6 – 12 nm) measurement. Equally excellent agreement is found between the SNOE Al/C (17 – 20 nm) and the rocket Al/Nb/C (17 – 21 nm) measurements. However, as mentioned above, these measurements are nearly a factor of two larger than the rocket Al/Sc/C (17 – 26 nm) measurement. The primary reason that the longer-wavelength photodiodes have small uncertainties and perhaps why the agreement is better (except with the Al/Sc/C photodiode) is that the ratios of the solar soft X-ray current to the solar visible current are largest for these photodiodes. The solar irradiances between 17 and 20 nm from the SNOE Al/C and the Al/Nb/C photometers indicate an agreement to within 2%. However, as discussed above, we suspect that the rocket Al/Nb/C photodiode irradiance might be too high. If this concern were ignored though, this comparison would indicate that the PTB BESSY and NIST SURF-II radiometric standards are in agreement and that there has been little or no degradation of the SNOE Al/C photodiode.

We feel that the comparisons between the SNOE and rocket measurements are, overall, very good and they serve as a validation for the SNOE measurements. A more careful analysis of the algorithms that remove the visible signal could improve the irradiance uncertainties for the SNOE photodiodes, and thus might improve the comparisons to the rocket measurements. Improvements for the visible light corrections for the rocket Ti/Pd, Ti/Zr/Au, and Al/Sc/C photodiodes might also improve these comparisons; however, the results from the other rocket photodiodes with similar bandpasses, but without the large visible light corrections, will not likely change with more detailed analysis. Alternatively, the higher values for the SNOE irradiances

could indicate that the sensitivities of the photodiodes or windows have changed since their calibrations. These soft X-ray photodiodes are expected to degrade ~1% percent per year, so it is difficult to explain how the sensitivities could have increased. The future comparisons of the SNOE solar measurements to the TIMED SEE satellite and underflight calibration measurements, possibly later in 2001, should be able to further validate the SNOE measurements and verify whether the photodiodes are stable over the long-term.

8. Conclusions

We have presented a time series of solar soft X-ray irradiance measurements made from the SNOE satellite. The measurements are made with a system of photometers that incorporate X-ray sensitive photodiodes with thin film coatings. These measurements cover 1.5 years beginning March 11, 1998. The 81-day average of the $F_{10.7}$ varied between 100 and 175 for this period. The irradiances show significant 27-day periodicity as well as a general rise to solar maximum. The magnitudes of the irradiances are shown to vary by factors of 4 to 8 over the time period of the SNOE data with the larger variability in the shorter wavelengths. The variability in the 81-day average for the time period is approximately a factor of 2 in all three wavelength channels. The average 27-day maximum to minimum ratios vary from 1.4 to 1.8 with again the larger variability at the shorter wavelengths. The data correlate very well with the Fl0.7 index. The technique used in analyzing the photometric data allows a ready comparison to the Hinteregger model of the solar soft X-ray irradiance. It is shown that the Hinteregger model underestimates the solar soft X-ray irradiance by approximately a factor of 4.0 at the moderate levels of solar activity seen by SNOE. The EUVAC model is in agreement with the SNOE measurements in the 6 - 19 nm range but underestimates the 17 – 20 nm irradiance by a factor of 1.8. The SOLAR2000 (version 1.03) model also underpredicts the solar irradiance in all three wavelength ranges by factors of ~3. On the basis of extrapolation of the SNOE data it is also shown that the SC#21REFW solar minimum reference spectrum, upon which the Hinteregger model is based, underestimates the solar minimum soft X-ray irradiance by approximately a factor of 2.5. The Hinteregger model underestimates the long-term variability in the solar soft X-ray irradiance by 20% in the 2 – 7 nm and 17 – 20 nm ranges and 60% in the 6 – 19 nm range over the time period of the SNOE mission. The empirical models all provide a reasonable representation of the 27-day periodicity. These results are consistent with other works that suggest that the solar soft X-ray irradiance is larger than the Hinteregger model. The SNOE measurements are compared with sounding rocket measurements using a similar technique. The sounding rocket instrument is the prototype for the TIMED SEE XUV Photometer System. While comparison with one of the rocket measurements is anomalous, the results indicate agreement to within uncertainties in the shortest wavelength channel and excellent agreement (within 2%) at the longer wavelengths.

Acknowledgments. The SNOE mission was managed by the Universities Space Research Association for NASA through the Student Explorer Demonstration Initiative. We acknowledge the contributions of the many students and professionals who contributed to the success of SNOE. We also thank W. Kent Tobiska for kindly providing the SOLAR2000 solar irradiance model predictions.

Janet G. Luhmann thanks W. Kent Tobiska and Douglas J. Strickland for their assistance in evaluating this paper.

References

Acton, L. W., D. C. Weston, and M. E. Bruner, Deriving solar X-ray irradiance from Yohkoh observations, *J. Geophys. Res., 104*, 14,827, 1999.

Bailey, S. M., C. A. Barth, M. J. Erickson, R. A. Kohnert, A. W. Merkel, E. M. Rodgers, S.C. Solomon, S. D. Straight, J. E. Vian, and T. N. Woods, Science instrumentation for the Student Nitric Oxide Explorer, *Proc. SPIE Int. Soc. Opt. Eng., 2830*, 264, 1996.

Bailey, S. M., T. N. Woods, L. R. Canfield, R. Korde, C. A. Barth, S. C. Solomon, and G. J. Rottman, Sounding rocket measurements of the solar soft X-ray irradiance, *Sol. Phys., 186*, 243, 1999a.

Bailey, S. M., T. N. Woods, C. A. Barth, and S. C. Solomon, Measurements of the solar soft X-ray irradiance from the Student Nitric Oxide Explorer, *Geophys. Res. Lett, 26*, 1255, 1999b.

Barth, C. A., W. K. Tobiska, D. E. Siskind, and D. D. Cleary, Solar-terrestrial coupling: Low latitude thermospheric nitric oxide, *Geophys. Res. Lett., 15*, 92, 1988.

Barth, C. A., S. M. Bailey, and S. C. Solomon. Solar-terrestrial coupling: Solar soft X-rays and thermospheric nitric oxide, *Geophys. Res. Lett, 26*, 1251, 1999.

Buansanto, M. J., S. C. Solomon, and W. K. Tobiska, Comparison of measured and modeled solar EUV flux and its effect on the E-F1 tegion of the ionosphere, *J. Geophys. Res., 97*, 10,513, 1992.

Canfield, L. R., New far UV detector calibration facility at the National Bureau of Standards, *App. Opt., 26*, 3831, 1987.

Canfield, L. R., J. Kerner, and R. Korde, Stability and quantum efficiency performance of silicon photodiode detectors in the far ultraviolet, *App. Opt., 28*, 3940, 1989.

Canfield, L. R., R. Vest, T. N. Woods, and R. Korde, *Proc. SPIE Int. Soc. Opt. Eng., 2282*, 31, 1994.

Feng, W. H. S. Ogawa, and D. L. Judge, The absolute solar Soft X-ray Flux in the 20 - 100Å region, *J. Geophys. Res., 94*, 9125, 1989.

Gibson, Sister Jean and J. A. Van Allen, Correlation of X-ray radiation (2-12A) with microwave radiation (10.7 centimeters) from the nonflaring Sun, *Astrophys. J., 161*, 1135, 1970.

Hinteregger, H. E., K. Fukui, and G. R. Gilson, Observational, reference and model data on solar EUV from measurements on AE-E, *Geophys. Res. Lett., 8*, 1147, 1981.

Judge, D. L., et al., First solar EUV irradiances obtained from SOHO by the CELIAS/SEM, *Sol. Phys., 177*, 161, 1998.

Kazachevskaya, T. V., S. I. Avdushin, D. A. Gonukh, A. I. Lomovsky, A. A. Nusinov, P. M. Svidsky, Yu. N. Tsigelnitsky, V. N. Oraevsky, I. M. Kopaev, and S. I. Boldirev, Solar flux and spectrum measurements in the EUV spectral region on board the CORONAS-I satellite, *Sol. Phys., 177*, 175, 1998.

Korde, R. and J. Geist, Quantum efficiency stability of silicon photodiodes, *App. Opt., 26*, 5284, 1987.

Korde, R., L. R. Canfield, and B. Wallis, Stable high quantum efficiency silicon photodiodes for vacuum-UV applications, *Proc. SPIE Int. Soc. Opt. Eng., 932*, 153, 1988.

Korde, R. and L. R. Canfield, Silicon photodiodes with Stable near theoretical quantum efficiency in the soft X-ray region, *Proc. SPIE Int. Soc. Opt. Eng., 1140*, 126, 1989.

Kreplin, R. W., The solar cycle variation of soft X-ray emission, *Ann. Geophys., 26*, 567, 1970.

Kreplin, R. W. and D. M. Horan, Variability of X-ray and EUV solar radiation in solar cycles 20 and 21, *Proceedings of the Workshop on the Solar Electromagnetic Radiation Study for Solar Cycle 22*, edited by R. F. Donnelly, p. 405, 1992.

Lean, J., Solar ultraviolet variations: A review, *J. Geophys. Res., 92*, 839, 1987.

Lean, J., A comparison of the sun's extreme ultraviolet irradiance variations, *J. Geophys. Res., 95*, 11,933, 1990.

Lean, J. Variations in the Sun's radiative output, *Rev. Geophys., 29*, 505, 1991.

Manson, J. E., The solar extreme ultraviolet between 30 and 205Å on November 9, 1971, compared with previous measurements in this spectral region, *J. Geophys. Res., 81*, 1629, 1976.

Ogawa, H. S., L. R. Canfield, D. McCullin, and D. L. Judge, Sounding rocket measurement of the absolute solar EUV flux utilizing a silicon photodiode, *J. Geophys. Res., 95*, 4291, 1990.

Ogawa, H. S., D. L. Judge, D. R. McMullin, and P. Gangopadhyay, First-year continuous solar EUV irradiance from SOHO by the CELIAS/SEM during 1996 solar minimum, *J. Geophys. Res.*, *103*, 1, 1998.

Richards, P. G., and D. G. Torr, An investigation of the consistency of the ionospheric measurements of the photoelectron flux and the solar EUV flux, *J. Geophys. Res.*, *89*, 5625, 1984.

Richards, P. G., and D. G. Torr, The altitude variation of the ionospheric photoelectron flux, A comparison of theory and measurement, *J. Geophys. Res.*, *90*, 2877, 1985.

Richards, P. G., J. A. Fennelly, and D. G. Torr, EUVAC: A solar EUV flux model for aeronomic calculations, *J. Geophys. Res.*, *99*, 8981-8992, 1994.

Siskind, D. E., C. A. Barth, and D. D. Cleary, The possible effect of solar soft X Rays on thermospheric nitric oxide, *J. Geophys. Res.*, *95*, 4311, 1990.

Siskind, D. E., D. J. Strickland, R. R. Meier, T. Majeed, and F. G. Eparvier, On the relationship between the solar soft X ray flux and thermospheric nitric oxide: An update with an improved photoelectron model, *J. Geophys. Res.*, *100*, 19,687, 1995.

Solomon, S. C., Optical aeronomy, *U. S. Natl. Rep. Int. Union Geod. Geophys. 1987-1990, Rev. Geophys.*, *29*, 1089, 1991.

Solomon, S. C., et al., The Student Nitric Oxide Explorer, *Proc. SPIE Int. Soc. Opt. Eng*, *2810*, 121, 1996.

Timothy, A. F. and J. G. Timothy, Long-term intensity variations in the solar helium II Lyman alpha line, *J. Geophys. Res.*, *75*, 6950, 1970.

Tobiska, W. K., Revised solar extreme ultraviolet flux model, *J. Atmos. Terr. Phys.*, *53*, 1005, 1991.

Tobiska, W. K. and C. A. Barth, A solar EUV flux model, *J. Geophys. Res.*, *95*, 8243, 1990.

Tobiska, W. K., and F. G. Eparvier, EUV97: Improvements to EUV irradiance modeling in the soft X-rays and FUV, *Sol. Phys.*, *177*, 147, 1998.

Tobiska, W. K., T. N. Woods, F. G. Eparvier, R. Viereck, L. Floyd, D. Bouwer, G. J. Rottman, and O. R. White, The Solar2000 empirical solar irradiance model and forecast tool, *J. Atmos. and Sol. Terr. Phys.*, in press, 2000.

Torr, M. R., and D. G. Torr, Ionization frequencies for solar cycle 21: Revised, *J. Geophys. Res.*, *90*, 6675, 1985.

Woods, T. N., F. G. Eparvier, S. M. Bailey, S. C. Solomon, G. J. Rottman, G. M. Lawrence, R. G. Roble, O. R. White, J. Lean, and W. K. Tobiska, TIMED Solar EUV Experiment, *Proc. SPIE Int. Soc. Opt. Eng*, *3442*, 180, 1998.

Woods, T. N., E. M. Rodgers, S. M. Bailey, F. G. Eparvier, and G. Ucker, TIMED Solar EUV Experiment: preflight calibration results for the XUV photometer system, *Proc. SPIE Int. Soc. Opt. Eng*, *3756*, in press, 1999.

S. M. Bailey, Center for Atmospheric Sciences, Hampton University, Hampton, Virginia 23668. (scott.bailey@hamptonu.edu)

C. A. Barth, S. C. Solomon, and T. N. Woods, Laboratory for Atmospheric and Space Physics, University of Colorado, Boulder, CO 80309-0590. (charles.barth@lasp.colorado.edu; stan.solomon@lasp.colorado.edu; tom.woods@lasp.colorado.edu)

L. R. Canfield, National Institute of Standards and Technology Physics Laboratory, Gaithersburg, MD, 20899-0001.

R. Korde, International Radiation Detectors, 2527 West 237th Unit B, Torrance, CA 90505-5243.

(Received May 23, 2000; revised July 27, 2000;
accepted July 27, 2000.)